



Simulation and Experiment Analysis of Driveshaft

Jia Hao Li^{1,*}, Yao Liu¹, Yang Zhou¹, You Zhe Wang¹, Zhan Ling Guo² and Bin Shen²

¹North University of China, Taiyuan, China

²Yangtze Delta Region Institute of Tsinghua University, Zhejiang, China

Abstract: A driveshaft is a small spring coil less than 1mm in diameter, composed of several stainless-steel wire filaments. In intervention, the driveshaft is used to transmit force and motion to the inside body through the existing micro channels (such as arteries, veins, and gastrointestinal tract). The performance of the driveshaft determines the efficiency, stability, and accuracy of force and motion transitions, the ability to pass through tortuous microchannels, and the damage to healthy tissues. To determine the influence of fabrication parameters (filament, wire diameter, and outer diameter) on the mechanical properties (such as bending stiffness and natural frequency) of the driveshaft, a simulation was established in ABAQUS to calculate the deformation displacement under 0.0098N and first-order natural frequency. Then, the bending stiffness is calculated. The results show that the bending stiffness and the first-order natural frequency of the driveshaft increase with the increase of the filament number and wire diameter, and with the outer diameter of the driveshaft increases, the bending stiffness increases, while the first-order natural frequency decreases. Finally, the simulation model is verified by measuring the deformation displacement in the experiment. This study provides a methodology for designing and selecting the driveshaft in interventional therapy.

Received on 03-07-2023
 Accepted on 15-08-2023
 Published on 30-08-2023

Keywords: Driveshaft, bending stiffness, natural frequency, fabrication parameters, simulation.

<https://doi.org/10.6000/2369-3355.2023.10.01>

1. INTRODUCTION*

The driveshaft is a component that intrudes into the human body, along the microchannel of the human being, to transfer the force and motion required for intervention. However, due to limitations of the microchannel (such as arteries and veins) size and tortuosity, the driveshaft has a small diameter (often less than 1 mm) and large length (often larger than 1300mm). The high length-to-diameter ratio makes the driveshaft much soft, which can easily cross the curved blood vessel. However, high stiffness is also needed to transfer the force and motion precisely. Additionally, the driveshaft in the heart and vascular system will be affected by the heart, respiration, blood, and complex human microchannels [1-3], causing deformation in the transmission process and blood vessel damage. Therefore, the mechanical property of the driveshaft is very important for the success of the intervention.

The existing research shows that the driveshaft deviation results from heart beating and the lack of blood vessel wall support in the heart [1, 2]. The accidental movement of the human cardiothoracic activity and external force intervention will cause the driveshaft to deviate from its predetermined

position. The accuracy of the device tissue interaction also depends largely on the driveshaft's effective and reliable mechanical properties [3-5]. In addition, the rigid driveshaft cannot adapt to the complex three-dimensional structure, so it will form complex injuries in the cardiac portal or coronary sinus, leading to extremely difficult tasks to operate on patients with arrhythmia (because of their irregular heartbeat) [6-8]. According to Fujiwara *et al.* [9], the size of the damage depends on the contact force, and the contact force may affect the stability of the driveshaft. In addition, The driveshaft is coated with hydrophobic, anti-corrosion, and anti-condensation coatings, which can realize anti-corrosion, wear resistance, and oxidation resistance [10]. Since the driveshaft is constantly bent in the operating environment, the interface between the coating and the driveshaft is subjected to shear and peeling forces, resulting in stress on the coating. Once the allowable stress of the coating material is exceeded, it will cause the coating to crack, flake, or damage. Coating shedding is the main wear form, which has a significant impact on the fracture strength of the driveshaft [11].

When the driveshaft front-end slides along the blood vessel, it will collide with the blood vessel wall and will often bend and deform to some extent [12]. If the driveshaft is deformed too much, it will scratch or puncture the blood vessel wall. At this time, a driveshaft with lower stiffness should be selected. If

*North University of China, Taiyuan, China; Tel: +8613152876986; E-mail: 1281720007@qq.com

the intracavitary device is large, a driveshaft with greater stiffness should be selected in order to allow the driveshaft to pass smoothly through the distal lesion path. When performing complex endovascular procedures, such as complex multi-stent vascular recanalization or the release of transplanted vessels, the high stiffness of the driveshaft ensures the integrity of the coating material and the corrosion and damage resistance of the driveshaft metal material [13]. Meanwhile, the influence of the operating frequency of the guide wire and other cooperating devices should be considered to avoid damage to blood vessels due to resonance. Therefore, in the actual environment of interventional surgery, the mechanical properties of the driveshaft are extremely important. So far, there are no detailed references on the effect of manufacturing parameters on the mechanical properties of the driveshaft.

In this study, the effects of different manufacturing parameters (filament, filament diameter, outer diameter) on the mechanical properties (bending stiffness and natural frequency) of the driveshaft were determined by establishing a simulation model in ABAQUS for displacement and deformation experiments and modal analysis of the driveshaft. Finally, the correctness of the finite element model is verified by experiments.

2. MATERIALS AND METHODS

2.1. Structural Model

As shown in Figure 1, the structure of the driveshaft is formed by several side-by-side wires wound around the mandrel. So, it can be defined by the wire diameter, filament number, mandrel diameter, and length.

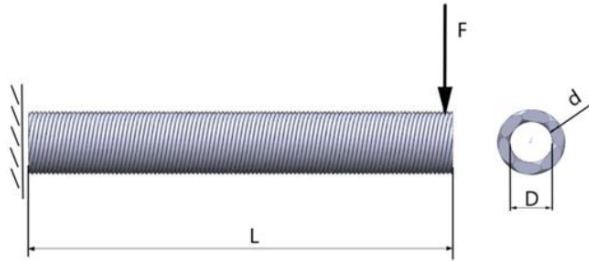


Figure 1: 3D Model Drawing.

Firstly, the driveshaft models are built in SolidWorks (2018, Dassault Systems) and saved in the format of IGES. Since the 304V wires are side-by-side, in theory, the contact surface between the adjacent wires is a line with zero thickness. In practice, there is a certain gap in the contact surface due to the extrusion or rebound between the wires. Therefore, in the finite element model, the clearance of the wire contact surface is set at 0.001mm, which is also reflected in the literature [14]. Then the model is imported into the finite element software ABAQUS (V2020, Dassault systems, France). Due to the geometric damage of the model caused by the change of the format, such as free edge,

repeat surface, etc., the finite element model is simplified and modified to obtain high-quality mesh elements [15, 16].

2.2. Selection of Simulation Parameters

The setting of material property parameters is one of the important factors affecting the analysis results. Setting the material performance parameters will affect the accuracy and reliability of the calculation results [17]. The driveshaft in the intervention is made by the 304V, which is the most used material in medicine. Table 1 gives the material properties of 304V [18], which has a density of 7900 kg/m³ and 195 MPa Young's modulus. The Poisson ratio is 0.25, and the failure stress is 197MPa. To consider the interaction among the wires in the deformation, the friction coefficient is given as 0.3.

Table 1: Material Properties of 304V Stainless Steel

Attribute	Numerical value
Material	304V
Density (kg/m ³)	7900
Young's modulus (Mpa)	195
Poisson ratio	0.25
Failure stress (Map)	197
Friction coefficient	0.3

After the material properties are given, the boundary and loading conditions are set. The left surface of the driveshaft is fixed. A 0.0098 N concentrated force is put on the right ending face to make the driveshaft bending. The gravity was applied on the whole driveshaft as a uniform force. The maximum incremental step is 100, which has an initial value of 0.1, and the minimum and maximum values are 1e-5 and 1, respectively.

The calculation time and results accuracy are affected by the grid size, type of elements, and quality [19]. The time of software calculation and the relationship between the accuracy of the calculation results and the number of grids is

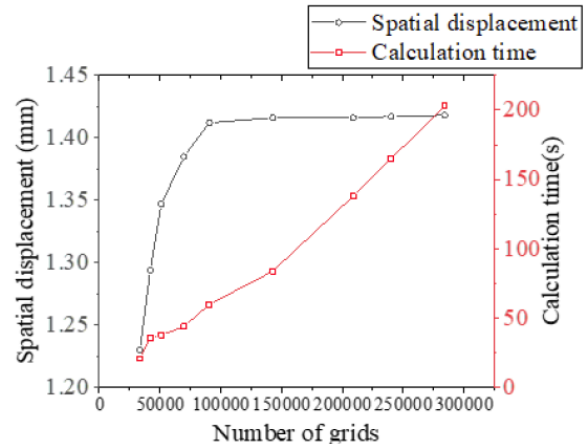


Figure 2: Calculate the Relationship between Time and Result Accuracy and The Grid.

shown in Figure 2. The calculation results are more accurate with the increase in the number of grids. However, when the number of grids reaches a certain level, the accuracy of the results will not be greatly improved; on the contrary, the consumed software calculation time will increase indefinitely.

According to the variation graph of the calculation results with the number of grids, when the number of grids reaches about 100000, the error of the calculation results will be controlled within 0.01 Mpa, and the time used is relatively short, which can achieve good efficiency. Therefore, considering the accuracy of the calculation results, the time of software calculation, and the computer performance, this research chooses the method of reducing the number of grids to speed up the software. Mesh the model under the MESH module of ABAQUS, and select the mesh size of 0.07 mm.

According to the piecewise analysis superposition method for calculating deflection in the mechanics of materials [20], in this study, the relationship between (deflection) spatial displacement and flexural stiffness is shown in Equation (1):

$$w_B = \frac{-Fl^3}{3EI} + \frac{-ql^3}{8EI} \quad (1)$$

The user-defined function is constructed in MATLAB (2020, MathWorks, USA), and its bending stiffness can be obtained through the displacement obtained from simulation analysis.

To sum up, the parameters of different driveshafts are set in the finite element software, as shown in Table 2.

Table 2: Simulation Parameters

Parameters	Value
Wire diameter, d (mm)	0.1, 0.15, 0.20, 0.25
Filament number, N	3, 4, 6, 8, 12
Mandrel diameter, D (mm)	0.3, 0.4, 0.5, 0.7
Length, l (mm)	15

2.3. Experimental Setup

To verify the simulation model of the driveshaft, the bending experiments were conducted to measure the displacement of the driveshaft under a certain weight. Figure 3 gives the configuration of the experiment setup. The driveshaft is fixed by the tape on the optical table; one of the driveshaft ends extends from the table boundary to a certain distance. Weight is connected to the driveshaft end to make it bend. The bending displacement was recorded by the rule behind the driveshaft.

In this study, the driveshaft used in the experiments is wound by 3 filaments of stainless steel wire. The wire diameter is 0.15 mm. The outside diameter of the driveshaft is 0.65 mm. The extension length from the optical table boundary is 15 mm, and the weight is 1 g.

After the experiments, the results are compared and analyzed with the simulation results to verify the accuracy and reliability of the simulation.

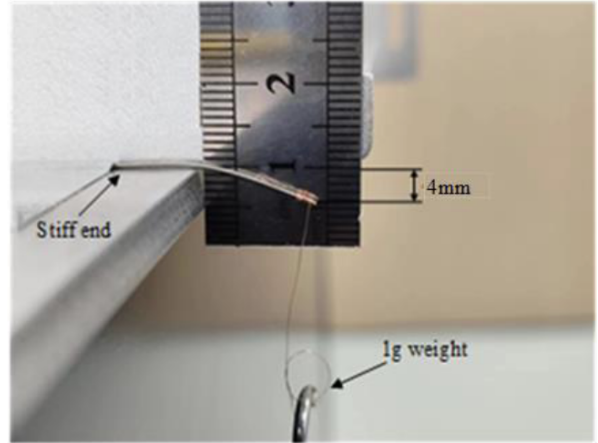


Figure 3: Schematic diagram of the experimental setup.

3. RESULTS AND DISCUSSION

The complete analysis type is selected in the operation module of ABAQUS software, and a multi-processor is used to solve the model. The simulation results get the cloud map of stress concentration and displacement distribution. The stress concentration area and displacement distribution in the model are shown in Figure 4.

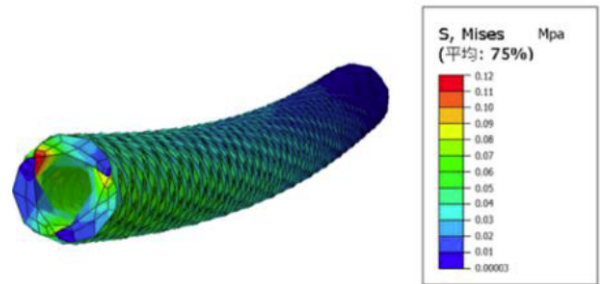


Figure 4: Stress Distributions.

3.1. Displacement and Bending Stiffness Analysis of Driveshaft

The bending stiffness is equal to the product of the elastic modulus E and the moment of inertia I of the beam section about the neutral axis. According to the basic beam theory, beam deflection is an index used to describe the degree of bending deformation along the beam axis after the beam is stressed. In the finite element analysis, under different mandrel diameters, the wire diameter and filament number of the driveshaft are changed, the space displacement under fixed external force is analyzed, and the bending stiffness is obtained by substituting the result into the deflection formula.

From Figure 5, the bending stiffness of the driveshaft increases with increased filament number and wire diameter for different mandrel diameters.

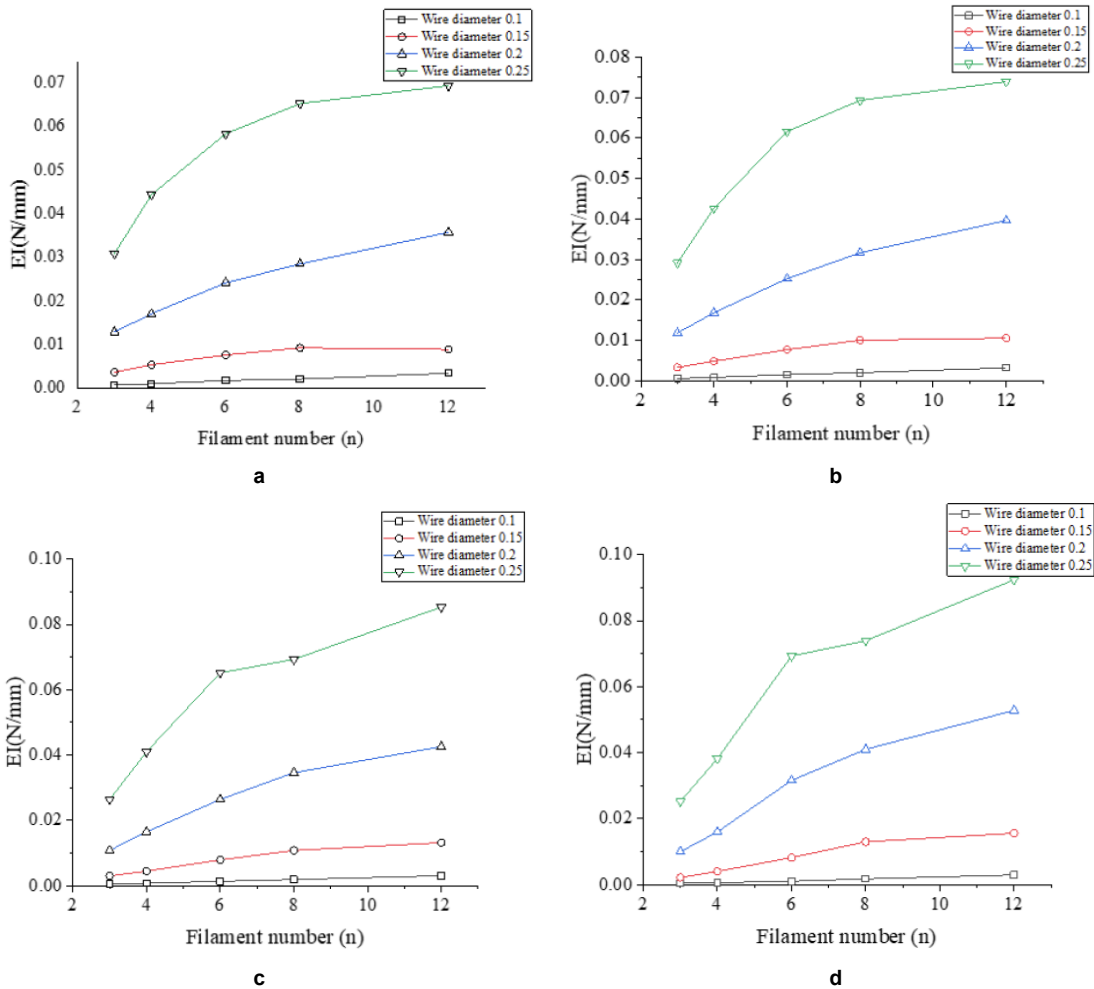


Figure 5: Influence of the wire diameter and filament number on the bending strength of the driveshaft at (a) 0.3, (b) 0.4, (c) 0.5, and (d) 0.7mm mandrel diameter.

Therefore, in the actual working environment, the driveshaft with suitable stiffness can be selected according to the complexity of vascular access and the actual situation of other co-working devices to ensure that the driveshaft can be competent for its work and avoid damage to the microenvironment in the body.

3.2. Modal Analysis

Modal analysis is a method to analyze structural dynamics. The modal analysis includes computational modal analysis and experimental modal analysis. The whole process of computational modal analysis is realized by the finite element method. The input and output signals of the system are obtained by the test method. The advantage of computational modal analysis is that the shape and size can be modified during the drawing design of the structure to reduce or avoid some unnecessary responses. The advantage of experimental modal analysis is that it can describe the vibration characteristics of the system through relevant modal parameters. Meanwhile, the system signal obtained in the computational modal analysis is input into the experimental modal analysis, which can modify and supplement the

original finite element model to verify whether the construction of the finite element model is reasonable.

The finite element software ABAQUS is used to analyze the constrained modes of the driveshaft when the number of filaments and the diameter of the steel wire change under different mandrel diameters. The vibration models and frequencies under the first-, second-, and third-order modes are obtained, as shown in Figures 6-8, which provides a basis for avoiding the resonance of the driveshaft and optimizing its parameter design.

In modal analysis, when the mandrel diameters are the same. The first-, second-, and third-natural frequencies of the driveshaft increase with the increase of the wire diameter and the number of filaments. The second-order natural frequency is approximately equal to the first-order natural frequency.

In general, the increase in mass (filament number) will reduce the modal frequency. In this study, the mass of the transmission shaft is unchanged, and the natural frequency and mode of each order under different stiffness are studied by analytical calculation in the simulation model. For an

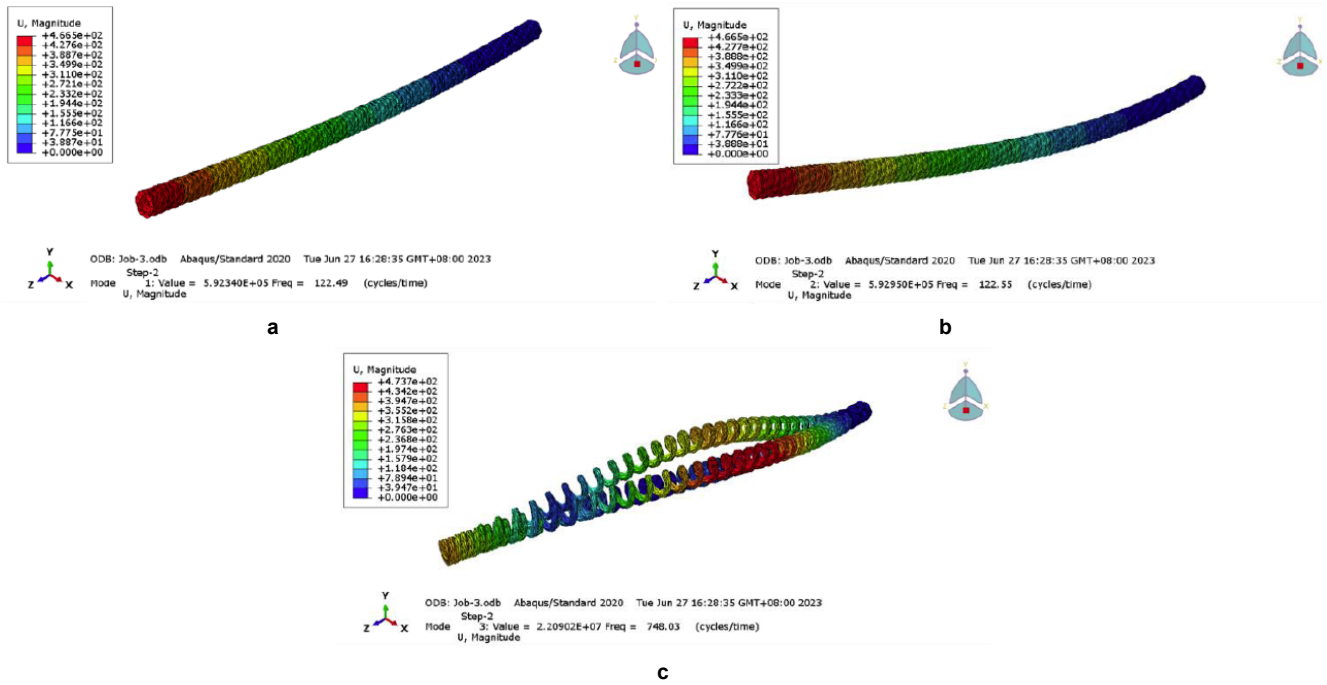


Figure 6: Vibration mode at (a) first-, (b) second, and (c) third-order-natural frequency.

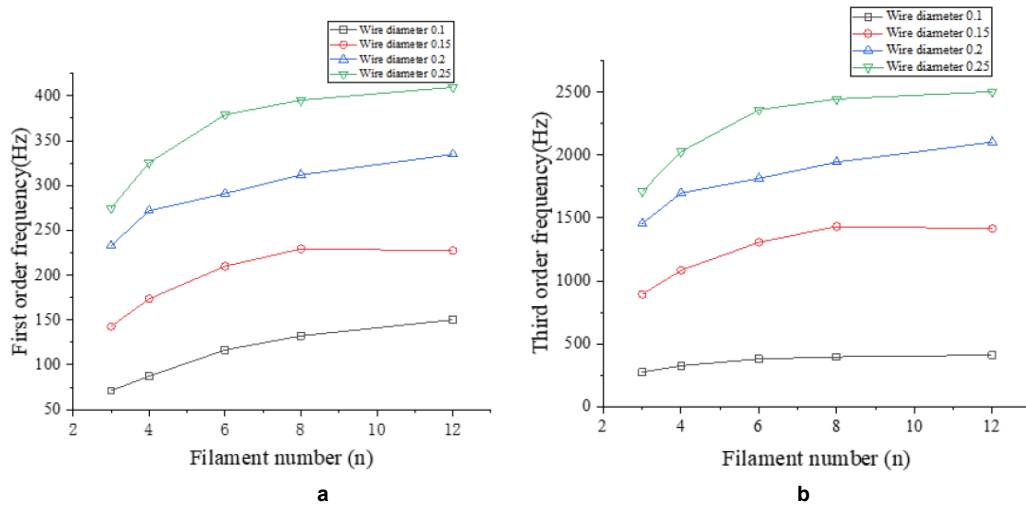


Figure 7: Natural frequency of first (a) and third (b) order at 0.3 mm mandrel diameter.

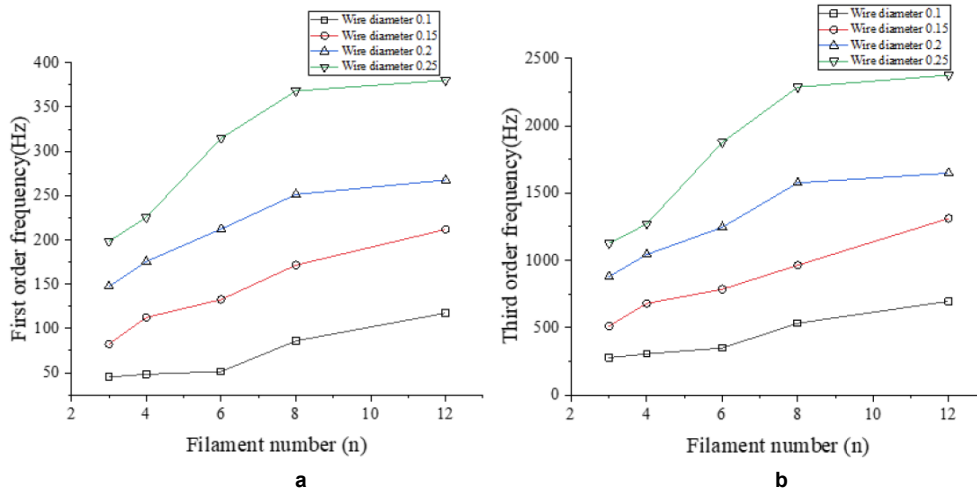


Figure 8: Natural frequency of first(a) and third(b) order at 0.7 mm mandrel diameter.

approximately cylindrical driveshaft, the M-order circumferential natural frequency can be expressed as [21]:

$$f_m = \frac{1}{2} \sqrt{\frac{K_m}{M_m}} \quad (2)$$

It can be concluded that the solid-state frequency of the driving shaft is not only related to its mass (the number of filaments) but also closely related to its stiffness. Therefore, it is necessary to consider the changes in mass and stiffness at the same time when studying the solid-state frequency. The mass of the driveshaft does not change, and the natural frequency of the driveshaft increases with the increase of stiffness.

3.3. Experimental Results

In this study, it is assumed that the driveshaft is a rigid material with negligible plastic deformation. For the setting of boundary conditions, the length of the driveshaft is specified as 15 mm, and the left end is fixed by the super glue tape. Mark the position points of the cardboard or the right end of the upper front and back for displacement measurements. The effect of assumptions and boundary conditions leads to some error between the actual measured displacement results and the results obtained from the simulation.

The displacement of the driving shaft under this parameter is about 4mm, as shown in Figure 3, which is less than 7% different from the displacement of 3.75mm in the simulation result (Figure 9). It can prove the accuracy of the simulation results.

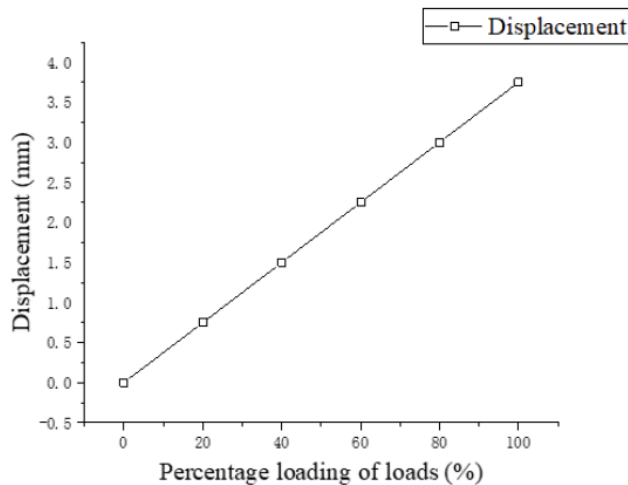


Figure 9: Simulation displacement result.

CONCLUSION

This paper focuses on the bending stiffness and vibration modes of driveshafts with different mandrel diameters when the number of filaments and filament diameter are changed. Through the study of the modeling of the transmission shaft, the shaft was calculated under the effect of different

manufacturing parameters of deformation and vibration frequency. And experimental measurements were introduced and compared with the simulation results. The conclusions can be drawn as follows:

1. According to the test results of displacement, after the bending stiffness analysis of the driveshaft, we have found that the bending stiffness of the driveshaft increases with the increase of the filament number and wire diameter under the condition of different mandrel diameters.
2. In the modal analysis, when the mandrel diameter is the same. The first-, second-, and third-order intrinsic frequencies of the driveshaft increase with the increase in wire diameter and filament number.
3. Further study of the modal analysis, we found that the intrinsic frequency of the driveshaft is not only related to its mass but also closely related to its stiffness. When the mass of the driveshaft is constant, the intrinsic frequency of the driveshaft increases with the increase in stiffness.
4. The error between the experimental measurements and the simulation results is less than 7%, which indicates that the simulation model is reliable.

In summary, with the wire diameter and shaft diameter as manufacturing parameters, using ABAQUS software simulation focuses on the influence of different parameters on the driveshaft stiffness and frequency, introduces the experiment verification, does our research for the shaft for the design of the transmission shaft and provide new insight into performance optimization. However, the current study may have limitations in terms of materials and other conditional constraints in practical applications. Future studies should more carefully consider the potential effects of material range, experimental methods, additional constraints, or other factors to understand better the behavior of driveshafts in real-world environments.

ACKNOWLEDGEMENTS

This research was supported by the Guangdong Provincial Key Laboratory of Minimally Invasive Surgical Instruments and Manufacture Technology (Granted No. MISIMT-2022-2) and Zhejiang Provincial Natural Science Foundation of China (Granted No. LY23E050002).

REFERENCES

- [1] Gerstenfeld EP. Contact force-sensing catheters – evolution or revolution in catheter ablation technology. *Circ Arrhythmia Electrophysiology* 2014; 7: 5-6. <https://doi.org/10.1161/CIRCEP.114.001424>
- [2] Lessick J, Karnowski R, Fuchs S, Ben-Hamite SA. Assessment of NOGA catheter stability during the entire cardiac cycle by means of a special needle-tipped catheter. *Catheter Cardiovasc Intern* 2001; 52(3): 400-406. <https://doi.org/10.1002/ccd.1090>

- [3] Klemm HU, Franzen O, Ventura R, Willems S. Catheter-based simultaneous mapping of cardiac activation and motion: a review. *Indian Pacing Electrophysiology J* 2007; 7(3): 148-159.
- [4] Fu Y, Liu H, Huang W, Wang S, Liang Z. Steerable catheters in minimally invasive vascular surgery. *Int J Med Robotics Compute Assist Surg* 2009; 5(4): 381-391. <https://doi.org/10.1002/ircs.282>
- [5] Lawanwong, Komgrit, Hamasaki, Hiroshi, Double-action bending for eliminating spring back in hat-shaped bending of advanced high-strength steel sheet. *International Journal of Advanced Manufacturing Technology* 2020; 106: 1855-1867.
- [6] Rafii-Tari H, Payne CJ, Yang GZ. Current and emerging robot-assisted endovascular catheterization technologies: a review. *Ann Biomed Eng* 2014; 42: 697-715.
- [7] Fujiwara R, Imamura K, Kijima Y, Masano T, Nagoshi R, Kohzuki A. The importance of catheter stability evaluated by Visitant during pulmonary vein isolation. *J Interv Card Electrophysiology* 2016; 2: 161.
- [8] Grunewald DE, Schmidt JA, Pendekanti R. Magnetic stabilization of catheter location sensor. *U.S. A1* 2007; 89: 32. <https://doi.org/10.1016/j.medengphy.2021.01.004>
- [9] Neumann T, Vogt J, Schumacher B, Dorszewski A, Kuniss M, Neuser H, *et al.* Circumferential pulmonary vein isolation with the cry balloon technique – Results from a prospective 3-center study. *J Am Coll Cardiol* 2008; 52(4): 278. <https://doi.org/10.1016/j.jacc.2008.04.021>
- [10] Xiang CY, Zhang FL, Wang J. Effect of particle size of nano-diamond on wear and corrosion resistance of electroless Ni-P composite coatings. *Diamond & Abrasives Engineering* 2021; 41(5): 14-20.
- [11] Chen SF, Wang CY, Zheng LJ. Cutting performance of diamond coated tools for machining graphite. *Diamond & Abrasives Engineering* 2021; 41(5): 70-76. <https://doi.org/10.13394/j.cnki.jgszz.2021.5.0012>
- [12] Ren LF, Mei C, Liu B. Image-based deformation modeling and force estimation of the front end of vascular interventional surgical apparatus 2022; 27(3):1001-1008.
- [13] Bai HQ, Zhong LS, Kang L. Fabrication of a novel molybdenum carbide composite coating with double-layer structure on cast iron via *in situ* solid-phase diffusion. *Materials Characterization* 2022; 183: 111613. <https://doi.org/10.1016/j.matchar.2021.111613>
- [14] Meneghetti G. Analysis of the fatigue strength of stainless steel based on the energy dissipation. *International Journal of Fatigue* 2007; 29(1): 81-94. <https://doi.org/10.1016/j.ijfatigue.2006.02.043>
- [15] Daniyan I, Mpofu K. Computer-aided simulation and performance evaluation of additive manufacturing technology for component parts manufacturing. *The International Journal of Advanced Manufacturing Technology* 2020; 107: 4517-4530. <https://doi.org/10.1007/s00170-020-05340-8>
- [16] Ghorbani H, Kim JH. Manufacturing of bent tubes with non-uniform curvature and cross-section using a novel hydroforming die: experimental, finite element analysis, and optimization. *International Journal of Advanced Manufacturing Technology* 2020; 107: 1683-1695. <https://doi.org/10.1007/s00170-020-05133-z>
- [17] Guo SH, Li J, Wang HT. Design parameters and modal optimization of radial vibration matching layer transducer. *Diamond & Abrasives Engineering* 2021; 41(6): 68-73. <https://doi.org/10.13394/j.cnki.jgszz.2021.6.0012>
- [18] Wang JQ, Song YT, Wu ST, Zhang YB. Structural design and optimization of cryostat feedthrough for ITER magnet. *Nuclear Techniques* 2006; 29(4): 271-275.
- [19] Cai LW. *Fundamentals of Mechanical Vibrations*. ASME-Wiley 2016; 317-330. <https://doi.org/10.1115/1.861FUNQ>
- [20] Schiro F. Modelling and analyzing the impact of hydrogen-enriched natural gas on domestic gas boilers in a decarbonization perspective. *Carbon Resources Conversion* 2020; 3: 122-129. <https://doi.org/10.1016/j.crcon.2020.08.001>
- [21] Wang DW, Yang W, Yang JF. Research on Electromagnetic Vibration Characteristics of a Permanent Magnet Synchronous Motor Based on Multi-Physical Field Coupling. *Chengdu Electric MFG* 2023; 16(9): 3916. <https://doi.org/10.3390/en16093916>

© 2023 Li *et al.*; Licensee Lifescience Global.

This is an open-access article licensed under the terms of the Creative Commons Attribution License (<http://creativecommons.org/licenses/by/4.0/>), which permits unrestricted use, distribution, and reproduction in any medium, provided the work is properly cited.